Journal of Sound and Vibration (1994) **176**(4), 515–529

NON-LINEAR RESPONSE OF PREDEFORMED PLATES SUBJECT TO HARMONIC IN-PLANE EDGE LOADING

J. R. MARÍN

Maritime Engineering and Sea Sciences, Escuela Superior Politécnica del Litoral, Guayaquil, Ecuador

N. C. PERKINS

Mechanical Engineering and Applied Mechanics, The University of Michigan, Ann Arbor, Michigan 48109-2125, *U.S.A.*

AND

W. S. VORUS

Naval Architecture and Marine Engineering, The University of Michigan, Ann Arbor, Michigan 48109-2125, *U.S.A.*

(*Received* 17 *March* 1992 *and in final form* 7 *May* 1993)

Following discretization, a non-linear ordinary differential equation of motion is obtained that describes the forced response of simply supported, predeformed plates. The excitation, which derives from harmonically varying in-plane edge loading, results in both external and parametric excitation. The equation of motion also includes the quadratic and cubic non-linearities associated with mid-plane stretching. Periodic solutions and their stability are determined by using the harmonic balance method. By varying the magnitude of predeformation, these solutions display two limiting types of behavior. Plate response is driven mainly through external excitation for "large" predeformation and mainly through parametric excitation for small predeformation. The solutions capture the interaction between parametric and external excitation for intermediate predeformation which causes a change in stability of one solution. This change in stability leads to an instability region for the limiting case of pure parametric excitation (vanishing predeformation).

1. INTRODUCTION

1.1. MOTIVATION

The presence of initial deformations in the plating of ship hulls is unavoidable. For example, plate waviness may result after the panels are welded to the stiffeners. This predeformation is identified herein as an important parameter affecting the dynamical characteristics of structures composed of plate elements. The present study is focused on the forced response of an (isolated) predeformed plate. The results derived for a single plate are applied to the vibration of ship hulls [1], and are the subject of a future publication.

1.2. RELATED STUDIES

Marguerre equations [2], sometimes also referred to as shallow shell equations, are often used in the analysis of predeformed plates. Coan [3] used an assumed series for the lateral

0022–460X/94/390515 + 15 $08.00/0 © 1994 Academic Press Limited

displacement to solve the compatibility equation; then, through a balance of the coefficients for the functions in the series, he obtained a set of algebraic equations for the amplitude of each term in the series. He used this approach to determine the static response of plates with small initial curvature loaded in edge compression. Yamaki [4] used a similar approach, but instead of balancing the coefficients, he applied the Galerkin method to discretize the equilibrium equations. Plates loaded statically in edge compression with various combinations of boundary conditions were treated by following this method.

Schultz [5] used the Coan–Yamaki approach to investigate the effect of initial deflections on the static performance of ship plating. He presented experimental results showing good agreement with analytical predictions. Jan [6], complemented Schultz's results by combining lateral and compression loads acting on the plate.

Cummings [7] studied the vibration of cylindrical shell segments under freely supported boundary conditions. He considered both free vibration and forced vibration due to an external lateral pressure. Somerset and Evan-Iwanowski [8] presented results of experiments with simply supported flat plates under parametric excitation. Leissa and Kadi [9] studied the effect of curvature upon the natural frequencies of shallow shells using the approach of Coan and Yamaki. They also incorporated the tangential inertia of the plate and found the influence to be small. Clamped rectangular plates under uniformly distributed lateral periodic loads were studied by Yamaki, Otomo and Chiba [10]. After the Coan–Yamaki approach was used to discretize the problem, the harmonic balance method was applied to solve a set of coupled Duffing equations. They also presented the results of experiments [11], confirming their computation. The effect of geometric imperfections on natural frequencies of simply supported flat plates under in-plane uniaxial and biaxial compression was studied by Hui and Leissa [12]. Hui [13] later considered laterally loaded plates and hysteretic damping. Ilanko and Dickinson [14] examined the linear vibration of simply supported, geometrically imperfect, rectangular plates. Their calculations, based on a Rayleigh–Ritz discretization, were corroborated by experimental results [15].

1.3. PRESENT STUDY

The objective of the present study is to examine the non-linear response of predeformed plates. Marguerre equations, altered to include plate inertia, are discretized by using the approach presented by Coan [3] and Yamaki [4]. The excitation considered is a distributed, harmonic, in-plane force acting on the edges of the plate. The combination of in-plane excitation and predeformation produces both external and parametric excitation terms in the governing equation of motion. Furthermore, the predeformation leads to quadratic non-linearities and to increases in the plate natural frequencies over those associated with and undeformed plate.

2. PROBLEM FORMULATION

The problem of interest is illustrated in Figure 1, and consists of an originally flat rectangular plate of width a and length b. The plate has simply supported edges along $y = \pm b/2$. Along $x = \pm a/2$, the edges remain simply supported for lateral deflections and are loaded by the average dynamic stress $p_x(t)$ for in-plane deflection. The plate predeformation is described by $w_0(x, y)$.

The Marguerre equations [2], sometimes also referred to as shallow shell equations, are used to study the dynamic response of predeformed plates. For this purpose, the static

lateral load is replaced by the plate inertia, so that the governing bending and in-plane equations, including the lateral predeformation of the plate, are

$$D[\partial^4 w/\partial x^4 + 2\,\partial^4 w/\partial x^2\,\partial y^2 + \partial^4 w/\partial y^4]$$
$$= -\rho\ddot{w} + h[F_{,yy}(w+w_0)_{,xx} - 2F_{,xy}(w+w_0)_{,xy} + F_{,xx}(w+w_0)_{,yy}]. \tag{1}$$

$$\partial^4 F/\partial x^4 + 2\,\partial^4 F/\partial x^2\,\partial y^2 + \partial^4 F/\partial y^4$$
$$= E[w_{,xy}^2 - w_{,xx}w_{,yy} + 2w_{0,xy}w_{,xy} - w_{0,xx}w_{,yy} - w_{0,yy}w_{,xx}], \tag{2}$$

where the plate flexural rigidity is $D = Eh^3/[12(1-\nu^2)]$ and E is Young's modulus, $F(x, y, t)$ is the Airy stress function, h is the plate thickness, $w(x, y, t)$ is the dynamic deformation of the plate measured from the predeformed state, $w_0(x, y)$ is the plate predeformation (unstressed state), ν is the Poisson ratio and ρ is the mass per unit area of the plate. The Airy stress function, F, is defined as

$$N_x/h = F_{,yy}, \qquad N_y/h = F_{,xx} \qquad \text{and} \qquad N_{xy}/h = -F_{,xy},$$

where N_x, N_y and N_{xy} are the components of the in-plane stress resultant in the indicated directions (force per unit length). These relations satisfy identically the two in-plane static equilibrium equations, when the in-plane inertia is negligible. This assumption, which will be employed here, follows the findings of Leissa and Kadi [9], who noted a very small reduction in natural frequency when the in-plane inertia is included.

The predeformed plate is simply supported on its four edges, and is assumed to be stress-free. Moreover, the predeformation of the plate is assumed to be

$$w_0(x, y) = hW_0 \cos(\pi x/a)\cos(\pi y/b), \tag{3}$$

which represents the leading term in a Fourier series expansion for general predeformation. W_0 is the (presumed known) amplitude of the predeformation expressed as a fraction of the plate thickness, h.

The associated boundary conditions are

$$w = 0 \quad \text{and} \quad M_y = 0 \quad \text{on } x = \pm a/2, \qquad w = 0 \quad \text{and} \quad M_x = 0 \quad \text{on } y = \pm b/2, \tag{4, 5}$$

$$N_{xy} = 0 \qquad \text{on} \quad x = \pm a/2 \quad \text{and} \quad y = \pm b/2, \tag{6}$$

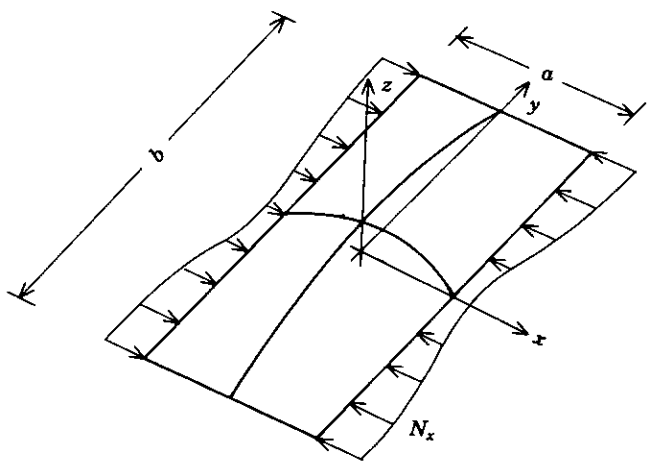

Figure 1. The predeformed plate geometry.

$$u^0(\pm a/2, y, t) = u^0(\pm a/2, t), \qquad v^0(x, \pm b/2, t) = v^0(\pm b/2, t), \tag{7, 8}$$

$$h\int_{-b/2}^{b/2} \sigma_x^0(\pm a/2, y, t)\,\mathrm{d}y = p_x(t)hb, \qquad h\int_{-a/2}^{a/2} \sigma_y^0(x, \pm b/2, t)\,\mathrm{d}x = 0. \tag{9, 10}$$

Here M_x and M_y are the bending moments per unit length about the x- and y-axes, respectively, $p_x(t)$ is the specified average dynamic in-plane stress applied along $x = \pm a/2$, σ_x^0 and σ_y^0 are the membrane stresses in the x- and y-directions, respectively, and u^0 and v^0 are the mid-surface displacements in the x- and y-directions, respectively. Conditions (7) and (8) require that the plate edges move uniformly in the x–y plane without distortion. The distribution of the in-plane displacement field is specified as uniform, but its magnitude cannot be specified *a priori*. Conversely, the distribution of in-plane membrane stresses cannot be specified, but its resultant (integral) can be specified as a prescribed function of time.

3. SOLUTION METHOD

The governing equations (1)–(10) are discretized following Coan [3] and Yamaki [4]. A one term separable solution for $w(x, y, t)$ is selected which satisfies the out-of-plane boundary conditions (4) and (5). Substitution into the in-plane equation (2) reduces it to a non-homogeneous biharmonic equation in the stress function F. The general solution, found in terms of particular and homogeneous solutions, is rendered unique through satisfaction of the remaining in-plane boundary conditions (6)–(10). Substitution of the stress function solution into the out-of-plane equation (1) and application of the Galerkin method results in a single non-linear ordinary differential equation of motion. Periodic solutions and their stability are determined by using the harmonic balance method.

A comparison function for $w(x, y, t)$ which satisfies the simply supported boundary conditions (4) and (5) is

$$w(x, y, t) = h\zeta(t)\cos(\pi x/a)\cos(\pi y/b), \tag{11}$$

where $\zeta(t)$ is a generalized co-ordinate. This choice is motivated by the fact that the (low frequency) dynamic deformation is likely to resemble the shape of the predeformation, given by equation (3). As with equation (3), equation (11) can also be interpreted as the leading term in a Fourier series expansion for general $w(x, y, t)$.

Substitution of equations (3) and (11) into equation (2) results in the non-homogeneous biharmonic equation

$$F_{,xxxx} + 2F_{,xxyy} + F_{,yyyy} = -Eh^2\zeta(\tfrac{1}{2}\zeta + W_0)(\pi^2/ab)^2[\cos(2\pi x/a) + \cos(2\pi y/b)].$$

The particular solution of this equation is

$$F_p = -(Eh^2/16)\zeta(\tfrac{1}{2}\zeta + W_0)[(1/\lambda^2)\cos(2\pi x/a) + \lambda^2\cos(2\pi y/b)], \tag{12}$$

where $\lambda = b/a$ is the plate aspect ratio.

By using the definitions of the non-linear membrane (mid-surface) strains [16], the midsurface displacement of the $x = a/2$-edge in the x-direction can be expressed as

$$u_p^0 = \int_0^{a/2} (\epsilon_x^0 - \tfrac{1}{2}w_{,x}^2 - w_{0,x}w_{,x})\,\mathrm{d}x,$$

where $\epsilon_x^0 = u_{,x}^0 + \tfrac{1}{2}w_{,x}^2 + w_{0,x}w_{,x}$ is the membrane strain in the x-direction. Substituting equation (12) in this expression, results in

$$u_p^0(a/2, y, t) = -(a/8)(h\pi/2)\zeta(\tfrac{1}{2}\zeta + W_0). \tag{13}$$

Similarly, the y-displacement of the $y = b/2$-edge is

$$v_p^0(x, b/2, t) = -(b/8)(h\pi/b)\zeta(\tfrac{1}{2}\zeta + W_0). \tag{14}$$

Equations (13) and (14) imply that the edges do not distort. As also $N_{xy} = hF_{,xy} = 0$, only the homogeneous solution of the stress function need be used to satisfy the remaining boundary conditions (9) and (10). The homogeneous solution

$$F_h = -p_x \cos(\omega t)(y^2/2) \tag{15}$$

includes an average in-plane stress, $p_x \cos(\omega t)$, representing the harmonic excitation in the x-direction, with frequency ω.

By using equations (12) and (15), the stress resltant $N_x = hF_{,yy}$ on the edges $x = \pm a/2$ is found to be

$$N_x = h\{E(h\pi)^2/4b^2\}\zeta(\tfrac{1}{2}\zeta + W_0)\lambda^2 \cos(2\pi y/b) - hp_x \cos(\omega t). \tag{16}$$

The first term in equation (16) guarantees straightness of the $x = \pm a/2$-plate edges, as required by equation (7). Note that the resultant (integrated) in-plane force remains $p_x hb$. In the case of free vibration, the second term in equation (16) vanishes. Thus, there is no resultant force on the plate edge, but the edge is not stress-free.

The complete solution for the stress function (12) and (15) and the expansion (11) for w are substituted into the bending equation (1). After applying the Galerkin method, the following ordinary differential equation is obtained for the generalized co-ordinate $\zeta(t)$:

$$\ddot{\zeta} + \omega_0^2[1 - 2\mu \cos(\omega t)]\zeta + \alpha\zeta^2 + \beta\zeta^3 = F \cos(\omega t). \tag{17}$$

Here:

$$\omega_0^2 = \frac{Eh^3\pi^4}{4\rho b^4}\left[\frac{(1+\lambda^2)^2}{3(1-\nu^2)} + \frac{W_0^2(1+\lambda^4)}{2}\right], \qquad \alpha = \frac{3Eh^3\pi^4(1+\lambda^4)W_0}{16\rho b^4}, \tag{18, 19}$$

$$\beta = \frac{Eh^3\pi^4(1+\lambda^4)}{16\rho b^4}, \qquad 2\mu\omega_0^2 = \frac{p_x h(\pi/a)^2}{\rho}, \qquad F = \frac{p_x h(\pi/a)^2 W_0}{\rho}. \tag{20–22}$$

Equation (17) captures the quadratic and cubic non-linearities associated with mid-plane stretching. The linear stiffness term is proportional to ω_0 which represents an approximate fundamental natural frequency for the one-term expansion (11). The terms $\zeta[2\mu\omega_0^2 \cos(\omega t)]$ and $F \cos(\omega t)$ capture, respectively, the parametric and external excitation created by the in-plane loading. 2μ is the ratio of the amplitudes of the average in-plane load p_x to the critical buckling load of the plate, $\sigma_{xcr}^0 = (\lambda + \lambda^{-1})^2\pi^2 D/b^2 h$.

The predeformation affects the response of the plate in three major ways.

1. It generates an external excitation. The combination of in-plane forces N_x and predeformation w_0 creates a vertical component of the in-plane force, denoted by $N_x w_{0,x}$ in Figure 2.

2. The predeformation generates a quadratic non-linearity. The first term in equation (16) captures the asymmetric response of the plate to lateral deflection ζ (see Figure 3). For $-2W_0 < \zeta < 0$, the central part of the plate (where the deformations are larger) experiences a compressive load which tends to drive the plate away from the predeformed position. This action is described by a quadratic non-linearity.

3. The predeformation stiffens the plate and increases the fundamental natural frequency.

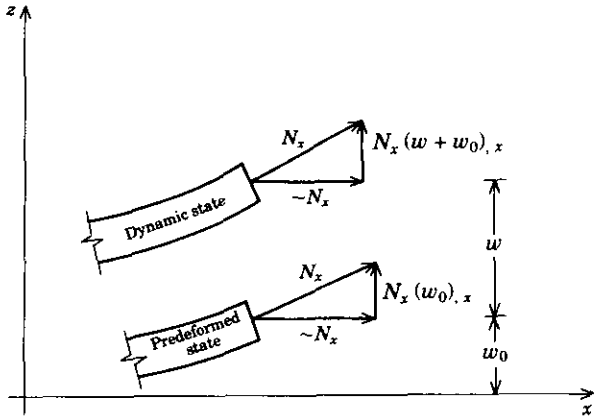

Figure 2. The source of external excitation.

4. REGIONS OF RESONANCE

For the linearized system, the parametric excitation in equation (17) produces unstable (unbounded) response for excitation frequencies $\omega \simeq 2\omega_0/n, n = 1, 2, 3, \ldots$ [17]. The first three instability regions are illustrated by the cross-hatched areas in the excitation frequency–amplitude plane of Figure 4 [17]. The largest region adjacent to $\omega = 2\omega_0$ is the region of principal parametric resonance. The non-linearities in equation (17) tend to bound the response and lead to large amplitude, resonant plate oscillations near these regions of dynamic instability.

The external excitation in equation (17) in combination with the non-linearities lead to primary ($\omega \simeq \omega_0$) and a number of secondary external resonances [18]. Subharmonic resonances exist for $\omega \simeq 2\omega_0$ and $\omega \simeq 3\omega_0$ and superharmonic resonances exist for $\omega \simeq \omega_0/2$ and $\omega \simeq \omega_0/3$. Note that the subharmonic $\omega \simeq 2\omega_0$, primary $\omega \simeq \omega_0$ and superharmonic $\omega \simeq \omega_0/2$ external resonances coincide, respectively, with the principal ($n = 1$), second order ($n = 2$), and fourth order ($n = 4$) parametric resonances.

These (severe) regions of combined resonance are considered in this analysis and are listed in Table 1. The first column indicates the approximate excitation frequency for each

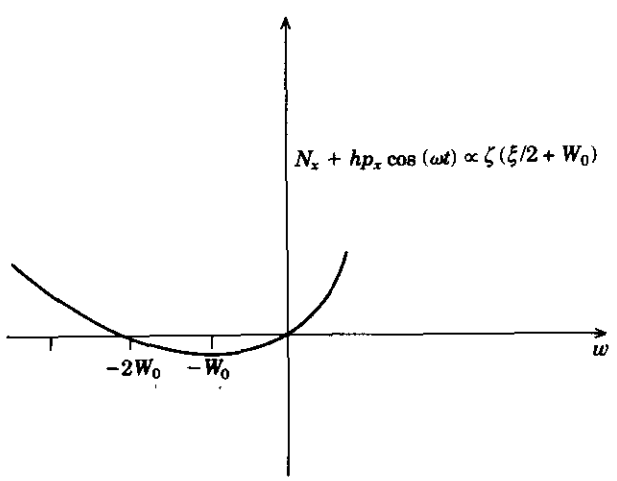

Figure 3. The source of quadratic non-linearity.

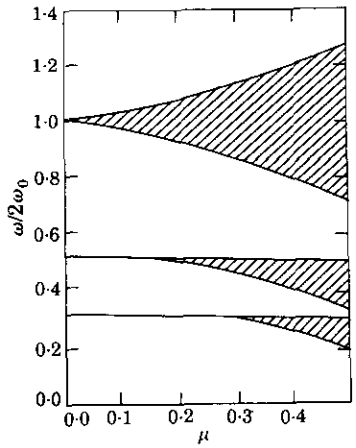

Figure 4. The first three regions of dynamic instability [17]. ω is the excitation frequency and ω_0 is the natural frequency.

region. The second and third columns indicate the parametric and external resonances associated with each region and the frequency of the harmonic component of the response in resonance.

The interaction between parametric and external excitation in the region of primary resonance ($\omega \simeq \omega_0$) was analyzed by HaQuang *et al.* [19], using the method of multiple scales [18]. In doing so, the parametric and external excitation were ordered at the first and second order levels, respectively. Thus the solution obtained cannot reproduce the response in the limiting case of pure external excitation.

In the present study, it is desired to have greater flexibility in assigning the relative importance of the parametric and external excitations. The amplitude of the external excitation (22) is proportional to the amplitude of the predeformation and ultimately dominates for cases of (relatively) large predeformation. Thus, a solution is sought that can capture the complete transition between pure parametric and pure external resonant response. For this purpose, the method of harmonic balance is adopted [17]. In the following, this method is used to determine periodic solutions and their stability throughout the frequency range encompassing the three regions of resonance shown in Table 1.

5. PRINCIPAL PARAMETRIC–SUBHARMONIC RESPONSE

In the principal parametric–subharmonic resonant region, the excitation frequency is approximately twice the plate natural frequency. The harmonic balance solution must

TABLE 1

Regions of combined resonance

Combined resonance region	Parametric resonance	External resonance
$\omega \simeq 2\omega_0$	Principal, $\omega/2$	Subharmonic, $\omega/2$
$\omega \simeq \omega_0$	Second order, ω	Primary, ω
$\omega \simeq \omega_0/2$	Fourth order, ω	Superharmonic, 2ω

therefore include a term with the frequency of the subharmonic resonance ($\omega/2$) as well as a term with the excitation frequency (ω) [17]: i.e.,

$$\zeta(t) = A\cos(\omega t/2) + B\sin(\omega t/2) + C\cos(\omega t) + D\sin(\omega t). \tag{23}$$

Here $A(t)$, $B(t)$, $C(t)$ and $D(t)$ represent slowly varying response amplitudes. The first two terms correspond to the principal parametric–subharmonic resonance, while the last two terms capture (possible) primary external response. Differentiating equation (23) twice leads to

$$\begin{aligned}\ddot{\xi} &= \ddot{A}\cos(\omega t/2) + \ddot{B}\sin(\omega t/2) + \ddot{C}\cos(\omega t) + \ddot{D}\sin(\omega t)\\ &- \omega\dot{A}\sin(\omega t/2) + \omega\dot{B}\cos(\omega t/2) - 2\omega\dot{C}\sin(\omega t) + 2\omega\dot{D}\cos(\omega t)\\ &- A(\omega^2/4)\cos(\omega t) - B(\omega^2/4)\sin(\omega t) - C\omega^2\cos(\omega t) - D\omega^2\sin(\omega t),\end{aligned}$$

where second order derivatives of the amplitudes are neglected, [17]. Substituting this result and equation (23) into equation (17) and equating coefficients of like harmonics leads to the following state equations governing the slowly varying amplitudes:

$$\dot{A} = \frac{1}{\omega}\left[B\left[\omega_0^2(1+\mu) - \frac{\omega^2}{4}\right] + \alpha(AD - BC) + 3\beta\frac{B}{2}\left[\frac{(A^2+B^2)}{2} + C^2 + D^2\right]\right], \tag{24}$$

$$\dot{B} = -\frac{1}{\omega}\left[A\left[\omega_0^2(1-\mu) - \frac{\omega^2}{4}\right] + \alpha(AC + BD) + 3\beta\frac{A}{2}\left[\frac{(A^2+B^2)}{2} + C^2 + D^2\right]\right], \tag{25}$$

$$\dot{C} = \frac{1}{2\omega}\left[D[\omega_0^2 - \omega^2] + \alpha AB + 3\beta\frac{D}{2}\left[\frac{(C^2+D^2)}{2} + A^2 + B^2\right]\right], \tag{26}$$

$$\dot{D} = \frac{1}{2\omega}\left[F - C[\omega_0^2 - \omega^2] - \alpha\frac{(A^2-B^2)}{2} - 3\beta\frac{C}{2}\left[\frac{(C^2+D^2)}{2} + A^2 + B^2\right]\right]. \tag{27}$$

The singular points of equations (24)–(27) satisfy the conditions $\dot{A} = \dot{B} = \dot{C} = \dot{D} = 0$ and provide the steady amplitudes for periodic solutions. The stability of each periodic solution is determined by linearizing equations (24)–(27) about the singular points and computing the eigenvalues of the resulting Jacobian matrix.

Closed form expressions for the periodic solutions are presently derived by using the approximation of Troger and Hsu, [20]. The steady state forms of equations (26) and (27) are linearized and provide the amplitudes for linear response:

$$C \approx F/(\omega_0^2 - \omega^2), \qquad D \approx 0. \tag{28, 29}$$

From the steady forms of equations (24) and (25), note that the trivial solution, $A = B = 0$, is always a solution.

With $X = \sqrt{A^2 + B^2}$ denoting the amplitude of the remaining (resonant) part of the solution, the steady forms of equations (24) and (25) provide two additional solutions:

$$X_1^2 = (4/3\beta)[(\omega^2/4)(1-\mu) + \alpha C + 3\beta C^2/2], \tag{30}$$

$$X_2^2 = (4/3\beta)[(\omega^2/4)(1+\mu) - \alpha C + 3\beta C^2/2]. \tag{31}$$

The solution (30) exists provided that $\omega > \omega_1$, where

$$\omega_1 = 2\sqrt{\omega_0^2(1-\mu) + \alpha C + 3\beta C^2/2}, \tag{32}$$

and solution (31) exists provided that $\omega > \omega_2$, where

$$\omega_2 = 2\sqrt{\omega_0^2(1+\mu) - \alpha C + 3\beta C^2/2}. \tag{33}$$

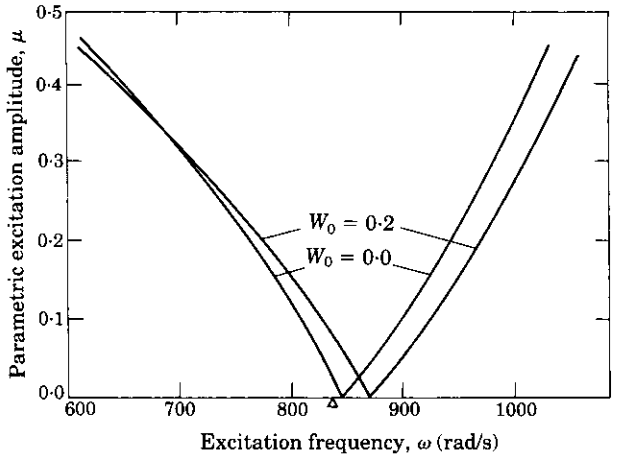

Figure 5. The influence of predeformation on the instability region for principal parametric resonance.

Note that in the limit of vanishing external excitation ($W_0 \to 0, F \to 0, C \to 0$), equations (32) and (33) reduce to the stability boundaries for principal parametric resonance reported by Bolotin [17]. These stability boundaries are altered by the (additional) external excitation considered herein.

The stability boundaries for the two cases of vanishing ($W_0 = 0$) and non-vanishing ($W_0 = 0{\cdot}20$) plate predeformation are illustrated in Figure 5. Inside the regions defined by the curves, the trivial solution ($X = 0$) is unstable and the plate oscillates laterally while being excited by the in-plane force. In this and all following examples we consider a steel plate with $E = 2{\cdot}113\,\mathrm{E}\ 10\,\mathrm{kg/m^2}$, $\nu = 0{\cdot}3$, $\rho g/h = 8\,\mathrm{gm/cm^3}$ (g being the gravitational acceleration $= 980\,\mathrm{cm/s^2}$), aspect ratio $b/a = 5{\cdot}00$, $a = 0{\cdot}762\,\mathrm{m}$ and thickness $h = 15{\cdot}32\,\mathrm{mm}$; these dimensions correspond to a deck plate of a large ship. The predeformation causes the instability region to shift to the right in response to the increased plate natural frequency (18). For the flat plate, the fundamental natural frequency, ω_0, is 417 1/s, and the buckling stress, $\sigma^0_{xcr} = 8{\cdot}35\,\mathrm{kg/mm^2}$. The predeformation also increases slightly the width of the instability region.

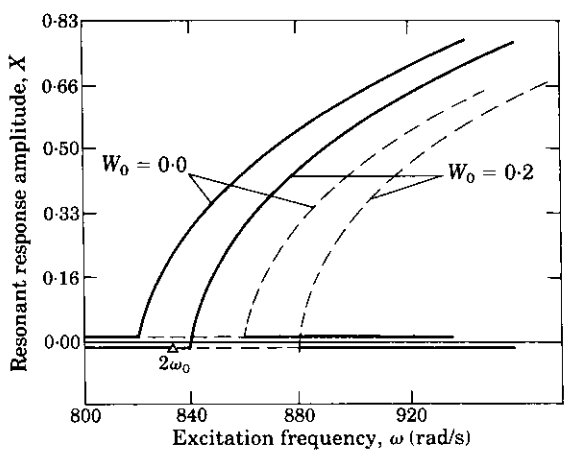

Figure 6. The principal parametric–subharmonic resonance. In this example, $\mu = 0{\cdot}05$.

In Figure 6, the (resonant) principal parametric–subharmonic amplitude, X, is plotted versus excitation frequency, for values of predeformation of 0·0 and 0·2. The solid and dashed curves denote stable and unstable periodic solutions, respectively. Solution stability is assessed as follows. Substituting $A = A^* + a(t)$ and $B = B^* + b(t)$ into equations (24) and (25), where A^* and B^* are the (steady) amplitudes of a periodic solution, leads to two autonomous state equations governing the perturbations $a(t)$ and $b(t)$. These variational equations are linearized and the eigensolutions are determined. Instability is indicated when any eigenvalue has a positive real part. This analysis reveals.that the trivial solution ($A^* = B^* = 0$) is unstable for $\omega_1 < \omega < \omega_2$ and is stable outside this region. Moreover, the solution $X = X_1$ is always stable (for $\omega > \omega_1$) while $X = X_2$ is always unstable (for $\omega > \omega_2$). Thus two stable periodic solutions coexist for $\omega > \omega_2$.

6. PRIMARY AND SUPERHARMONIC RESONANCE REGIONS

Responses in the primary superharmonic and external resonance regions are analyzed with one formulation. The harmonic balance solution must include terms with the superharmonic frequency (2ω), the harmonic frequency (ω), and a constant term as discussed in reference [17]:

$$\zeta(t) = A\cos(2\omega t) + B\sin(2\omega t) + C\cos(\omega t) + D\sin(\omega t) + S, \tag{34}$$

The constant term captures the possible vibration drift generated by the quadratic non-linearity [18]. Again, the quantities $A(t)$, $B(t)$, $C(t)$, $D(t)$ and $S(t)$ represent slowly varying response amplitudes. As shown below, this assumed solution form captures the evolution of the response associated with the primary external resonance region ($\omega = \omega_0$) to that associated with the superharmonic resonance region ($\omega \approx \omega_0/2$).

By following the procedure outlined in section 5, the resultant amplitude state equations are found to be

$$\dot{A} = (1/4\omega)\{D\mu\omega_0^2 + B(\omega_0^2 - 4\omega^2) + \alpha(2BS + CD) + 3\beta[(BA^2/4) + (BD^2/2) + (BC^2/2) + BS^2 + CDS + (B^3/4)]\}, \tag{35}$$

$$\dot{B} = -(1/4\omega)\{C\mu\omega_0^2 + A(\omega_0^2 - 4\omega^2) + \alpha(2AS + (C^2/2) - (D^2/2)) + 3\beta[(AB^2/4) + (AD^2/2) + (AC^2/2) - (SD^2/2) + (SC^2/2) + AS^2 + (A^3/4)]\}, \tag{36}$$

$$\dot{C} = (1/2\omega)\{B\mu\omega_0^2 + D(\omega_0^2 - \omega^2) + \alpha(BC - AD) + 3\beta[(DB^2/2) + (DA^2/2) + (DC^2/4) + DS^2 - ADS + BCS + (D^3/4)]\}, \tag{37}$$

$$\dot{D} = (1/2\omega)\{F + \mu\omega_0^2(A + 2S) - C(\omega_0^2 - \omega^2) - \alpha(BD + AC + 2CS) - 3\beta[(CB^2/2) + (CA^2/2) + (CD^2/4) + (CS^2/2) + BDS + ACS + (C^3/4)]\}, \tag{38}$$

$$-\mu\omega_0^2 C + S\omega_0^2 + \alpha[S^2 + \tfrac{1}{2}(A^2 + B^2 + C^2 + D^2)] + 3\beta[(AC^2/4 - (AD^2/4) + (SB^2/2) + (SA^2/2) + (SD^2/2) + (SC^2/2) + S^3] = 0. \tag{39}$$

The singular points of equations (35)–(39) are determined by simultaneous solution for the conditions $\dot{A} = \dot{B} = \dot{C} = \dot{D} = 0$. Solution was first attempted by using standard Newton–Raphson iteration. This procedure, however proved to be very time demanding and was not always successful. In particular, many combinations of initial guesses would converge to the same root, or simply not converge at all. Greater success followed from

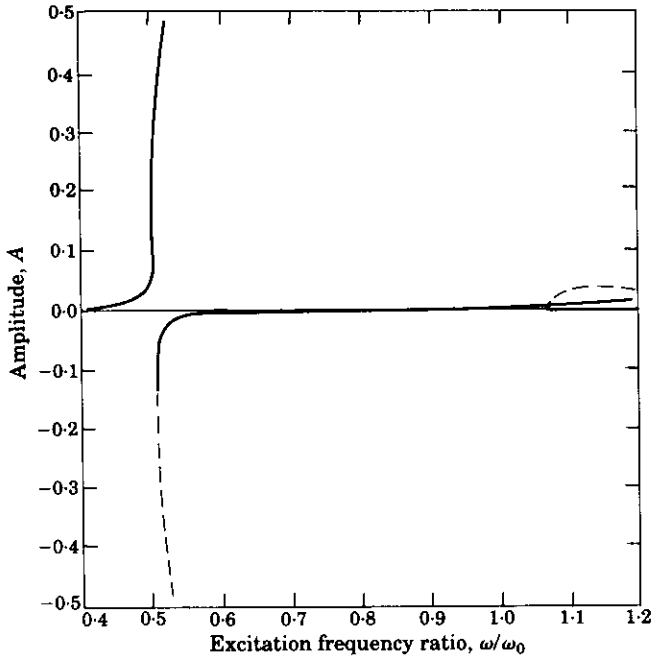

Figure 7. The superharmonic cosine amplitude ($W_0 = 0{\cdot}20$, $\mu = 0{\cdot}05$).

using the so-called continuation method [21]. Starting from a known root, this method follows the solution branch by using a predictor–corrector scheme. The solution branches were parameterized by using an arc length co-ordinate. For the predictor, fourth-order Runge–Kutta integration was employed, and for the corrector Newton–Raphson iteration was used.

In Figures 7 and 8 are shown the amplitudes of the cosine superharmonic (2ω), A, and cosine harmonic (ω), C, respectively, as functions of the excitation frequency. The amplitudes of the corresponding sine terms are zero. In this example, $W_0 = 0{\cdot}20$ and $\mu = 0{\cdot}05$. Two resonances occur over the indicated frequency range: (1) the superharmonic at, approximately, $\omega = \omega_0/2$; and (2) the primary at approximately $\omega = \omega_0$. Stable and unstable solution branches are denoted by the solid and dashed curves, respectively. The stability of the solution changes at the turning points. Furthermore, the solution branches all bend to the right, indicative of a hardening type non-linearity. For the case considered, the softening effect of the quadratic non-linearity is overshadowed by the stiffening effect of the cubic non-linearity.

From Figure 8 for the harmonic cosine amplitude, C, observe the strong interaction of the solution branches in the two resonance regions. In particular, the stable solution branch originating near the superharmonic resonance, $\omega \approx \omega_0/2$, is continuous with a stable solution branch at the principal external resonance region, $\omega \approx \omega_0$. Note also that, in this example with relatively large predeformation ($W_0 = 0{\cdot}20$), the response near $\omega \approx \omega_0$ is dominated by the external excitation.

The influence of the plate predeformation is further investigated by examining the response near the limit $W_0 \to 0$. At this limit, the external excitation vanishes and the plate is subjected to pure parametric excitation. Thus, the region near $\omega \approx \omega_0$ must evolve from one associated with primary external resonance to one associated with second order parametric resonance; refer to Table 1.

This evolution is highlighted in Figure 9, which illustrates solutions for the two cases $W_0 = 0{\cdot}01$ and $W_0 = 0{\cdot}001$ in the region $\omega \approx \omega_0$. As before, $\mu = 0{\cdot}05$ is used. The following observations are made.

1. Notice the appearance of the harmonic sine term D in Figure 9(b). This term, which appears only for cases of small predeformation, is indicative of the growing influence of the parametric excitation. The solution branches for D are all unstable and the point where they cross the frequency axis, P_1 for $W_0 = 0{\cdot}01$ and P_2 for $W_0 = 0{\cdot}001$, converges to one boundary of the instability region in the limiting case of pure parametric excitation ($W_0 \to 0$).

2. As the predeformation decreases, the two solutions of the harmonic cosine term, C, migrate towards each other; refer to Figure 9(a). Their limiting position ($W_0 \to 0$) defines the lower boundary of the parametric instability region. In this limit, they also approach the frequency axis signaling the fact that the trivial solution is a solution for the case of pure parametric excitation.

3. The stability characteristics of the negative solution branch of the harmonic cosine term, C, are altered. In these two examples, stability is exchanged at the points marked $P_1(W_0 = 0{\cdot}01)$ and $P_2(W_0 = 0{\cdot}001)$ as well as at the turning points marked $V_1(W_0 = 0{\cdot}01)$ and $V_2(W_0 = 0{\cdot}001)$. Stability is lost at the points P_1 and P_2 through a Hopf bifurcation.

4. In the limiting case of pure parametric excitation, the point P migrates towards the frequency axis in Figure 9 and passes through the turning point to the upper portion of the (negative) solution branch for C. Thus, as in the case $W_0 = 0{\cdot}001$, an unstable region exists between the points marked P_2 and V_2. This instability region converges to the frequency axis in the limit of vanishing W_0 where it becomes the instability region for second order parametric resonance.

These findings are summarized in Figure 10, which shows the complete evolution between externally driven response ("large" W_0) to parametrically drive response ($W_0 \to 0$).

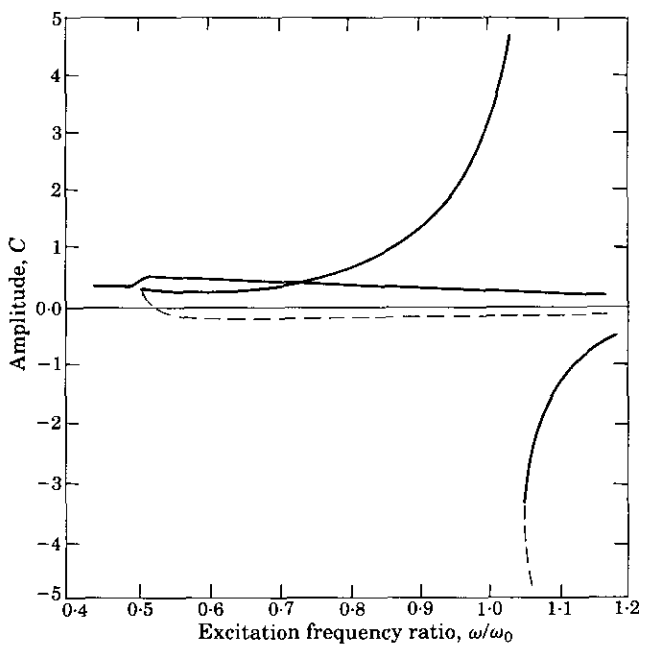

Figure 8. The harmonic cosine amplitude, C ($W_0 = 0{\cdot}20$, $\mu = 0{\cdot}05$).

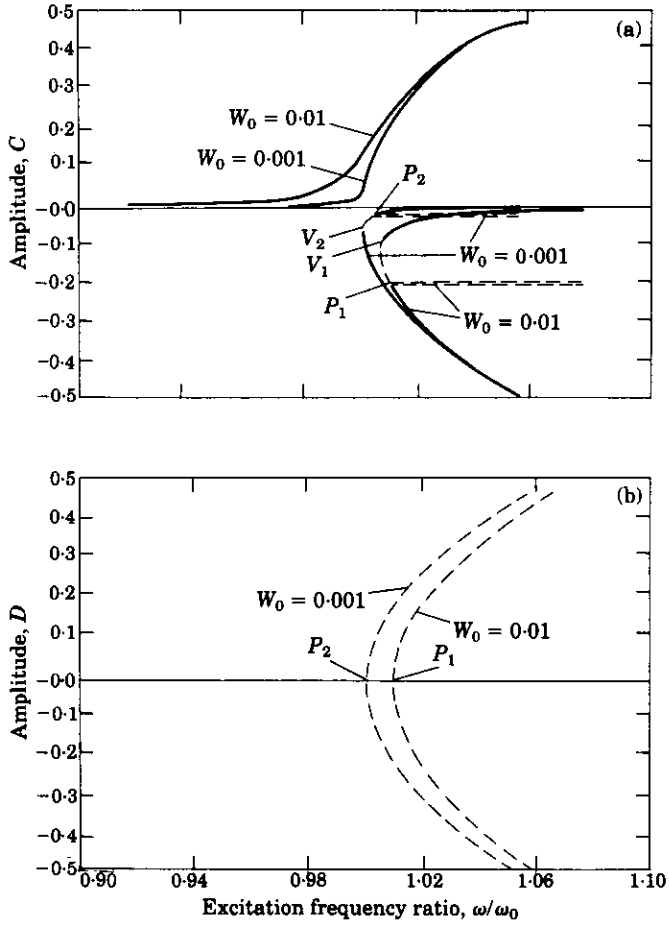

Figure 9. The amplitudes of the harmonic terms C (a) and D (b) for the response near $\omega = \omega_0$. Solutions are shown for $W_0 = 0{\cdot}01$ and $0{\cdot}001$. In both cases, $\mu = 0{\cdot}05$.

The amplitudes of the harmonic terms, C and D, are plotted in the excitation frequency/predeformation plane near resonance $\omega/\omega_0 = 1{\cdot}0$.

Qualitatively similar results were obtained by Ness [22] and by Hsu and Cheng [23], for systems with combined parametric and external excitation, the first in the case of a differential equation with negative cubic non-linearity, and the second in the case of linear differential equations.

7. CONCLUSIONS

Plate predeformation introduces first order (linear) coupling of in-plane and lateral response. This coupling results in externally excited lateral response for predeformed plates subjected to in-plane loading. Moreover, predeformation leads to a small increase in the fundamental plate natural frequency and generates a quadratic non-linearity describing mid-plane stretching.

The predeformation significantly alters the character of the resonances associated with combined external and parametric excitation. In particular, the response near $\omega \approx \omega_0$ is dominated by primary external resonance for (relatively) large predeformation W_0. In the limit of vanishing predeformation, the response near $\omega \approx \omega_0$ is dominated by a second

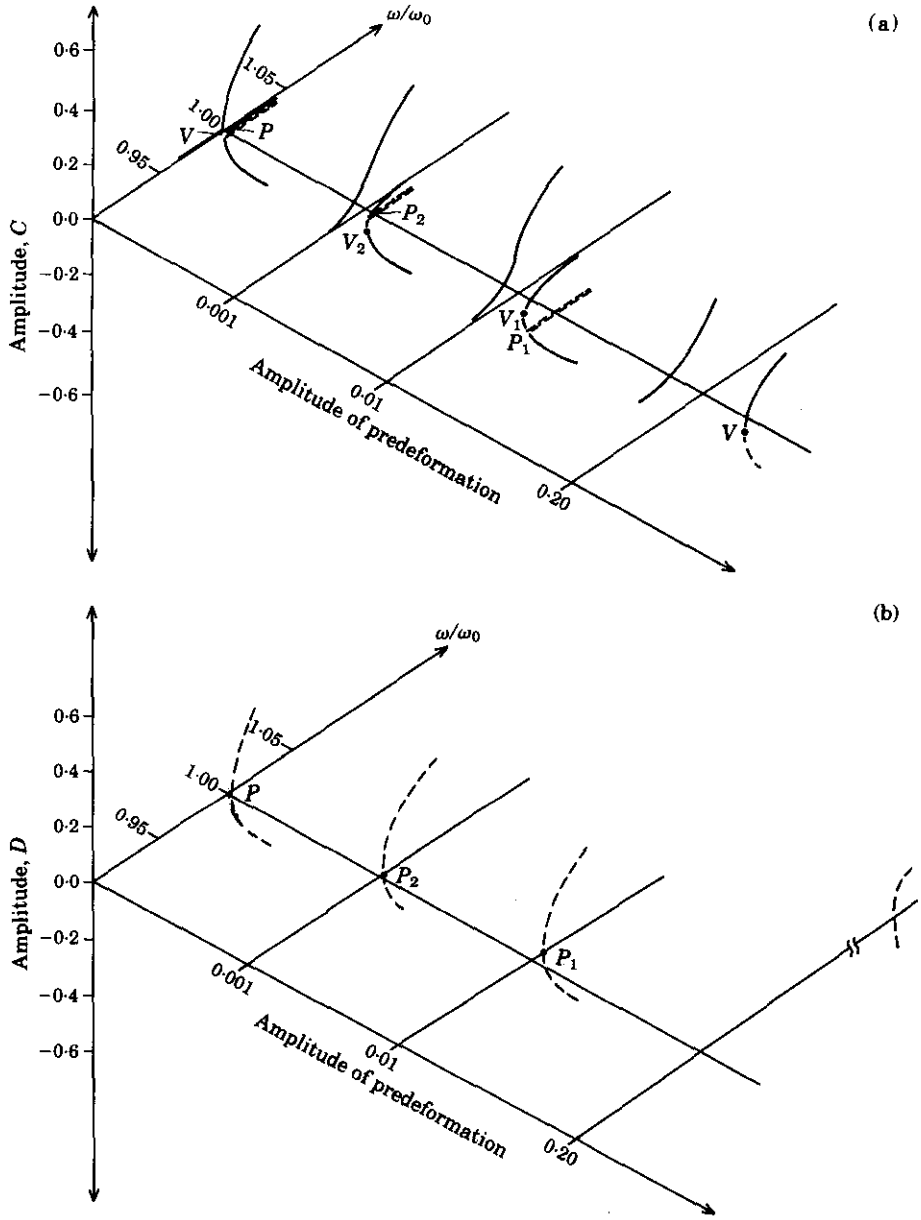

Figure 10. The evolution of the solution branches between mostly externally excited ("large" predeformation) to purely parametrically excited (no predeformation). (a) Amplitude C; (b) amplitude D.

order parametric resonance. The transition between these two limiting cases follows from the change in stability of one branch of the periodic solutions.

REFERENCES

1. J. R. MARÍN 1990 *Ph.D. Thesis, Department of Naval Architecture and Marine Engineering, The University of Michigan, Ann Arbor, Michigan.* Influence of initial imperfections of plating on the vibration of ship hulls.

2. K. MARGUERRE 1938 *Proceedings of the Fifth International Congress for Applied Mechanics, Cambridge*. Zur Theorie der Gekrummten Platte Grosser Formanderung.
3. J. M. COAN 1951 *Journal of Applied Mechanics*, 143–151. Large-deflection theory for plates with small initial curvature loaded in edge compression.
4. N. YAMAKI 1959 *Journal of Applied Mechanics* 407–414. Postbuckling behavior of rectangular plates with small initial curvature loaded in edge compression.
5. H.-G. SCHULTZ 1964 *Effect in Initial Deflection on Ship Plating Performance under Compression—Theory and Experiment*. University of California at Berkeley: Institute of Engineering Research.
6. H.-Y. JAN 1965 *Wide Ship Plating with Small Initial Deflection under Edge Compression and Lateral Load*. University of California at Berkeley: Office of Research Services.
7. B. E. CUMMINGS 1964 *American Institute of Aeronautics and Astronautics* **2**, 709–716. Large-amplitude vibration and response of Curved Panels.
8. J. H. SOMERSET and R. M. EVAN-IWANOWSKI 1966 *Developments in Theoretical and Applied Mechanics* **3**. Experiments on large amplitude parametric vibration of rectangular plates.
9. A. W. LEISSA and A. S. KADI 1971 *Journal of Sound and Vibration* **16**, 173–187. Curvature effects on shallow shell vibrations.
10. N. YAMAKI, K. OTOMO and M. CHIBA 1983 *Thin Walled Structures* **1**, 3–29. Nonlinear vibrations of a clamped rectangular plate with initial deflection and initial edge displacement, Part I: Theory.
11. N. YAMAKI, K. OTOMO and M. CHIBA 1983 *Thin Walled Structures* **1**, 101–109. Nonlinear vibrations of a clamped rectangular plate with initial deflection and initial edge displacement, Part II: Experiment.
12. D. HUI and A. W. LEISSA 1983 *Journal of Applied Mechanics* 750–756. Effects of geometric imperfections on vibrations of biaxially compressed rectangular flat plates.
13. D. HUI 1984 *Journal of Applied Mechanics* 216–220. Effects of geometric imperfections on large-amplitude vibrations of rectangular plates with hysteresis damping.
14. S. ILANKO and S. M. DICKINSON 1987 *Journal of Sound and Vibration* **118**, 313–336. The vibration and post-buckling of geometrically imperfect simply supported rectangular plates under uni-axial loading, part I: theoretical approach.
15. S. ILANKO and S. M. DICKINSON 1987 *Journal of Sound and Vibration* **118**, 337–351. The vibration and post-buckling of geometrically imperfect simply supported rectangular plates under uni-axial loading, part II: experimental investigation.
16. CH.-Y. CHIA 1980 *Nonlinear Analysis of Plates*. New York: McGraw-Hill.
17. V. V. BOLOTIN 1964 *The Dynamic Stability of Elastic Systems*. San Francisco: Holden-Day.
18. A. H. NAYFEH and D. T. MOOK 1979 *Nonlinear Oscillations*. New York: Wiley-Interscience.
19. N. HAQUANG, D. T. MOOK and R. H. PLAUT 1987 *Journal of Sound and Vibration* **118**, 425–439. A non-linear analysis of the interactions between parametric and external excitations.
20. H. TROGER and C. S. HSU 1977 *Journal of Applied Mechanics* 179–181. Response of a nonlinear system under combined parametric and forcing excitation.
21. R. SEYDEL 1988 *From Equilibrium to Chaos*. New York: Elsevier.
22. D. J. NESS 1971 *Journal of Applied Mechanics* 585–590. Resonance Classification in a Cubic system.
23. C. S. HSU and W.-H. CHENG 1974 *Journal of Applied Mechanics* 371–378. Steady-state response of a dynamical system under combined parametric and forcing excitations.